Journal of Structural Geology, Vol. 14, No. 10, pp. 1267 to 1275, 1992
Printed in Great Britain

0191-8141/92 $05.00+0.00

A strain model for antithetic fabric rotation in shear band structures

P. STOCK

Geologisches Institut, J. W. Goethe-Universität, D-6000 Frankfurt am Main, Germany

(*Received* 15 *May* 1991; *accepted in revised form* 11 *May* 1992)

Abstract—A numerical strain model based on infinitesimal strain theory is presented which simulates the progressive deformation and rotation of a foliated microlithon. It can be shown that an antithetical rotation of the microlithon's foliation with respect to the bulk sense of shear is a geometric consequence of specified strain conditions. The application of the model to asymmetric shear band structures described from the Gurktal Nappe, Eastern Alps, reveals that even the internal foliation of these structures must have been rotated antithetically. This corresponds with rare field observations and supports the suitability of asymmetric shear band structures as indicators for the local sense of shear.

INTRODUCTION

THE idea to investigate the strain history of shear band structures by means of computer modelling arose during field work in the southern Gurktal Nappe, Eastern Alps (Stock 1989). In this area, shear band structures as shown in Fig. 1 are the most frequent asymmetric structures indicating non-coaxial strain.

Asymmetric shear band structures originate from a non-coaxial deformation with both stretching and shearing components parallel to a pre-existing foliation (Platt 1979, 1984, Platt & Vissers 1980, Harris & Cobbold 1984, Hanmer 1986). The general suitability of asymmetric shear band structures as indicators for the bulk sense of shear is still being discussed (Passchier 1984, Behrmann 1987). The most common interpretation is, however, that both the bulk sense of shear on the external foliation and the sense of shear on the shear bands are identical (in Fig. 1 they are all dextral). If this assumption holds true, the internal foliation between the shear bands must have been rotated antithetically. The question is thus which strain geometry (homogeneous/heterogeneous, pure shear/simple shear, etc.) gives rise to these antithetical fabric rotations.

The theoretical and mathematical fundamentals of the present paper are the theory of strain partitioning (Means *et al.* 1980, Lister & Williams 1983), the tensor calculus and Mohr equations for infinitesimal plane strain (Means 1976, Ramsay & Huber 1983) and the equations for infinitesimal rigid-body rotation (Ghosh & Ramberg 1976).

BASIC APPROACH

After initial development of shear bands, the deformation of shear band structures is heterogeneous and even discontinuous. For the purpose of analysis of this deformation path a strain model is needed that gives a sufficient solution to the problem but that nevertheless is based on a simple and reliable approach.

Following Lister & Williams (1983), a state of homogeneous infinitesimal strain is usually determined by rate of stretching, shear-induced vorticity, spin and rate of translation. Essential for any strain description is the chosen reference frame. In the case of a planar structure such as a foliation, the complete strain can even be described by partitioning into a pure shear component and a simple shear component parallel to the foliation, and into rates of rotation and translation of the foliation (Fig. 2).

In Fig. 2(a), the foliation is still a passive marker and the deformation is homogeneous on any scale. In Fig. 2(b), however, the foliation causes the strain partitioning. It consists of numerous foliation sheets which are separated by discrete shear planes, and the simple shear component itself is further partitioned into discrete slips between the single foliation sheets. On a small scale this is still a bulk homogeneous simple shear but on a large scale the deformation is now heterogeneous. Within the sheets the deformation is pure shear because the shear-induced vorticity is reduced to zero.

The examples in Fig. 2 illustrate two extremes in straining a pre-existing foliation. In reality, a superposition of both strain types is expected to take place with a reduction of the shear-induced vorticity in the less deformable layers and an increase in the more deformable layers (respectively a discrete slip on foliation-parallel shear planes). The bulk strain will not be affected by this strain partitioning but deformation energy will be minimized especially when deformation changes from ductile to brittle. The partitioning of simple shear into discrete slips parallel to a pre-existing planar structure is expected before a corresponding partitioning even of the pure shear component because potential angular and conjugate shear planes (e.g. shear bands) still do not exist.

To describe the approximate deformation of a single asymmetric shear band structure, an elliptic foliated microlithon is chosen (Fig. 3). It is defined by its ellipticity ($R = a/b$) and by the orientation of its long axis (θ_a). External and internal foliations (s_e, s_i) are passive markers to fix the reference frame (X–Y) and to illus-

SG 14:10-J

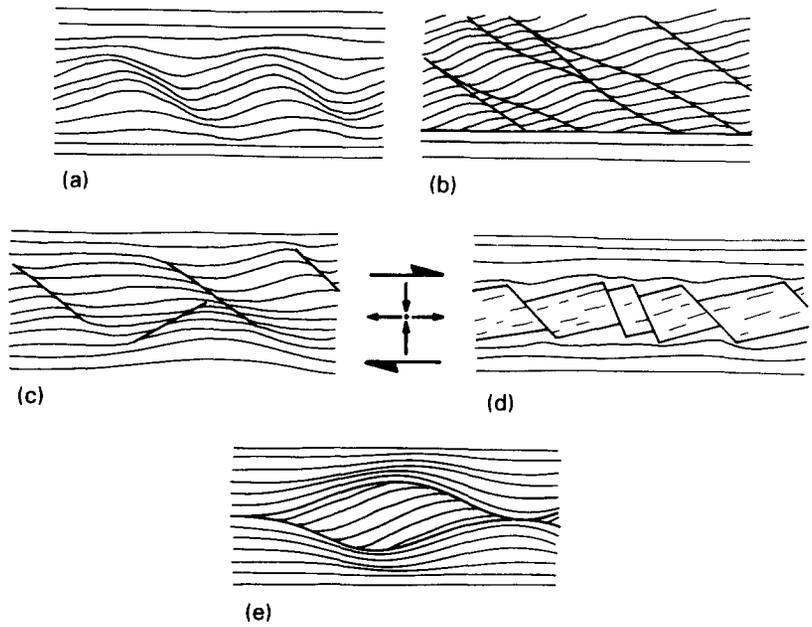

Fig. 1. Asymmetric shear band structures with a dextral sense of shear. (a) Extensional crenulation cleavage. (b) Multiple shear bands. (c) Conjugate shear bands. (d) Boudinage with rigid microlithons. (e) Foliation fish.

trate the internal fabric rotation. The unconstrained matrix is homogeneously deformed by combined rates of simple and pure shear (γ_x', ε_x') with a variable strain-type ratio ($S_r = \varepsilon_x'/\gamma_x'$). Since the reference frame is fixed to the external foliation, translation and spin of the foliation are set to zero.

The microlithon shall be completely separated from the matrix by a non-cohesive surface. The relative deformability (D) of the microlithon is variable in relation to the matrix: It is rigid for $D = 0$ (100% rigid-body rotation) and it is as deformable as the matrix for $D = 1$ (100% deformation). The modified strain rate tensor ($\mathbf{L}_i'$) for the deformation of the microlithon is:

$$\mathbf{L}_i' = D\mathbf{L}' = D\begin{pmatrix} \varepsilon_x' & \gamma_x' \\ 0 & -\varepsilon_x' \end{pmatrix}, \qquad (1)$$

where $\mathbf{L}'$ is the strain rate tensor for the matrix deformation. The modified equation of Ghosh & Ramberg (1976) for the microlithon's rigid-body rotation is:

$$\theta_\alpha' = (1 - D)\left(\varepsilon_x' \frac{R^2 - 1}{R^2 + 1} \sin 2\theta_a + \gamma_x' \frac{R^2 \cos^2\theta_a + \sin^2\theta_a}{R^2 + 1}\right), \qquad (2)$$

where θ_a' is the rate of rigid-body rotation. It results from integrating all single surface rotation rates of the tensor $(1 - D)\,\mathbf{L}'$ over the microlithon's complete surface. It is important to mention here that especially in the case of small ellipticities rigid-body rotation needs inhomogeneous matrix deformation to ensure strain compatibility. Rigid bodies with large ellipticities ($R > 10$),

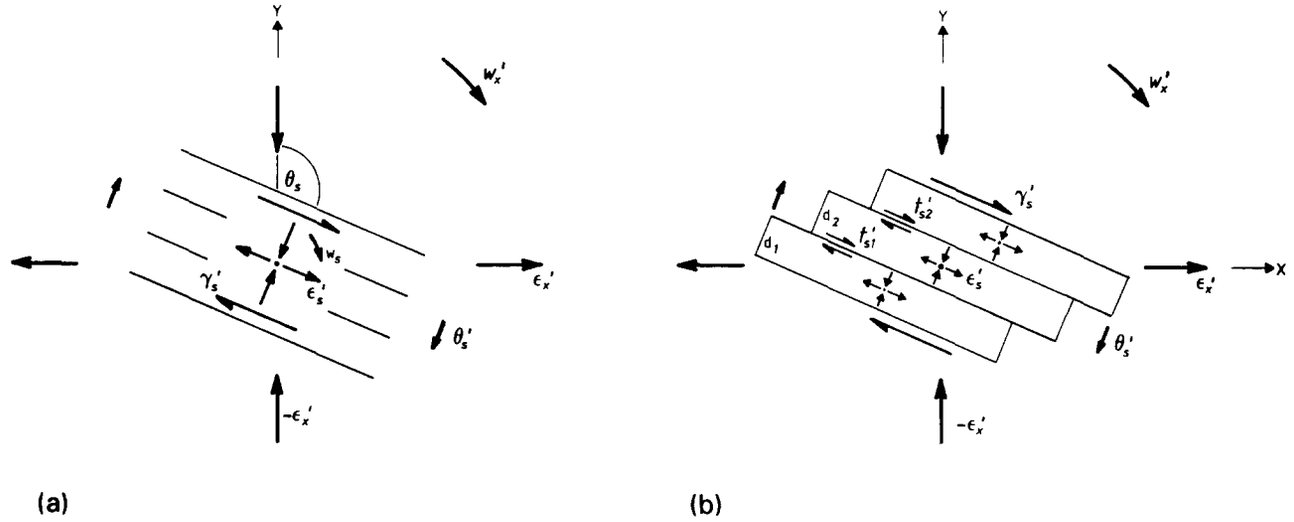

Fig 2. Strain partitioning by a pre-existing foliation. (a) The external strain (ε_x', w_x') is partitioned into spin (θ_s'), simple shear (γ_s'; with shear-induced vorticity, $w_s' = \gamma_s'$) and pure shear (ε_s'). (b) The simple shear is additionally partitioned into discrete translations (t_{sn}') and the internal shear-induced vorticity is reduced to zero.

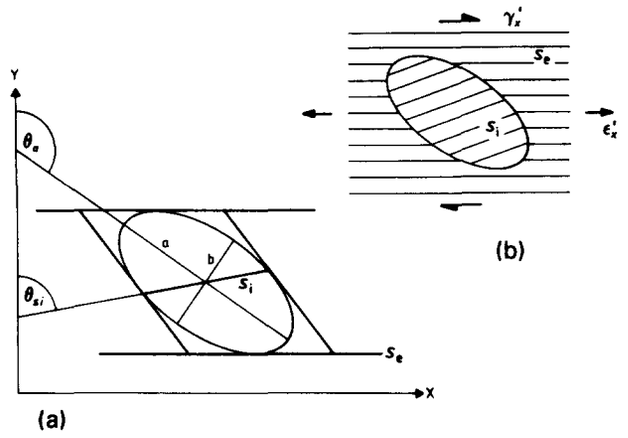

Fig. 3. Simplified model for the deformation of a shear band structure. (a) The cross-section of a single microlithon is assumed to be elliptic; ellipticity, $R=a/b$; ellipse orientation, θ_a; orientation of the internal foliation, θ_{si}. (b) The matrix is marked by the external foliation (s_e), the microlithon is marked by the internal foliation (s_i) and the bulk strain is partitioned into dextral simple shear (γ_x') and extensional pure shear (ε_x').

however, rotate approximately like passive markers and will hardly affect matrix deformation.

According to the above considerations about strain partitioning in the presence of non or less cohesive structures, the internal deformation of the microlithon may be of two opposite types. The first internal strain type is a homogeneous non-coaxial one with the same principal strain axes and the same strain-type ratio (ε_x'/γ_x') as the external bulk strain (Fig. 4a). Only the strain amounts may be reduced according to the relative deformability of the microlithon. The spin (θ_{si}') of the internal foliation is then:

$$\theta_{si}' = \theta_a' + D\,(\varepsilon_x' \sin 2\theta_{si} + \gamma_x' \cos^2\theta_{si}), \qquad (3)$$

where θ_{si} is the orientation of the foliation.

The opposite internal strain type is a coaxial one (Fig. 4b) with only a pure shear component (ε_{ai}') left. Its principal strain axes are parallel to the ellipse axes and rotate with the spin (θ_{ai}'):

$$\varepsilon_{ai}' = D\,(\tfrac{1}{2}\gamma_x' \sin 2\theta_a - \varepsilon_x' \cos 2\theta_a) \qquad (4a)$$

$$\theta_{ai}' = D\,(\gamma_x' \cos^2\theta_a + \varepsilon_x' \sin 2\theta_a). \qquad (4b)$$

The corresponding simple shear component (γ_{ai}') parallel to the long axis is set to zero because it is taken to be compensated by discrete slips on the long sides of the ellipse. So the spin of the internal foliation (θ_{si}') is:

$$\theta_{si}' = \theta_a' + \theta_{ai}' - \varepsilon_{ai}' \sin 2(\theta_{si} - \theta_a). \qquad (4c)$$

The complete internal deformation is heterogeneous because otherwise it would not be compatible to the ellipse deformation prescribed by equation (1). Coaxial deformation can only take place in the ellipse's central part where its long sides are approximately parallel to the ellipse and strain axes. At the ellipse's ends, however, deformation must be non-coaxial for the internal strain to remain balanced.

Equations (1)–(4c) are the basic equations to investigate the antithetical rotation of the microlithon's internal foliation. Equation (1) yields the rate of deformation of the microlithon, equation (2) yields its rate of rigid-body rotation, equation (3) yields the spin of the internal foliation in homogeneous non-coaxial strain and equation (4c) yields the same spin in heterogeneous but centrally coaxial strain. In reality, a combination of equations (3) and (4c) is most likely and equation (4c) may become more relevant in discribing cases with increasing ellipticities.

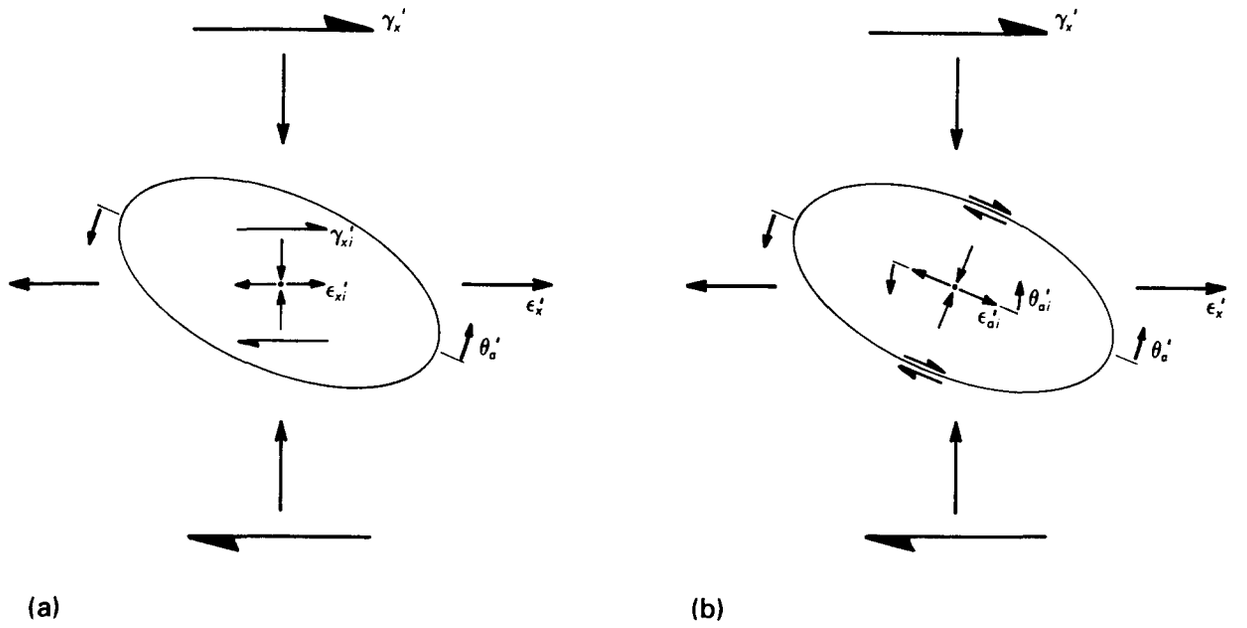

Fig. 4. Strain partitioning by an elliptic microlithon. The bulk strain is partitioned into rigid-body rotation (θ_a') and internal deformation. (a) Non-coaxial internal deformation with identical internal and external strain axes. (b) Coaxial internal deformation with identical internal strain and ellipse axes; the shear-induced vorticity is compensated by discrete slips on the long sides of the ellipse.

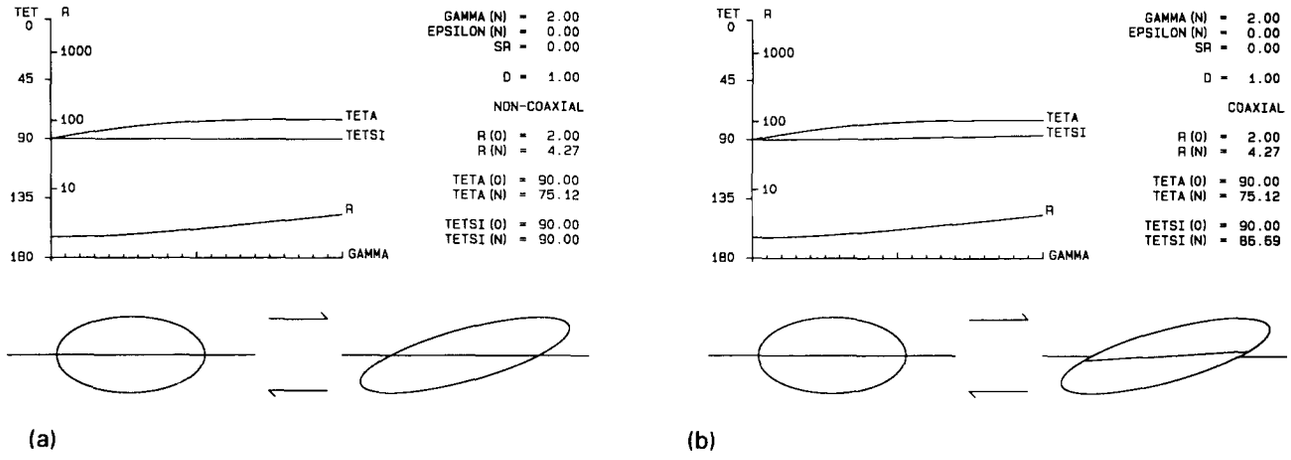

Fig. 5. Simple shear deformation of an incompetent microlithon. (a) Non-coaxial internal deformation. (b) Coaxial internal deformation. (θ_a = TETA, θ_{si} = TETSI.)

NUMERICAL APPLICATION: PROGRESSIVE DEFORMATION

In order to simulate the progressive deformation and rotation of the foliated microlithon, numerical application is used. Starting with initial values for ellipticity and orientation, the calculation gives their final values after a finite bulk strain of the matrix. For this purpose a time-related finite-difference method is used with the finite strain (γ_x, ε_x) being subdivided in numerous finite increments ($\Delta\gamma_x = \gamma_x'$ $\Delta t <= 0.001$, $\Delta\epsilon_x = \varepsilon_x'$ $\Delta t <= 0.001$). For these small increments the equations (1)–(4c) are still valid and can be used in a numerical algorithm of a BASIC program called PROGDEF. (Listings and discettes are available with the author.)

Each pass through this algorithm yields the results of one increment of matrix deformation. At first, the new ellipticity and the new orientation of the microlithon are calculated using the ellipse equation $(Ax^2 + Bxy + Cy^2) = 1$. In a following step, the incremental rigid-body rotation of the microlithon is calculated and added to its former orientation. And, finally, the incremental rotation of the foliation is calculated and added to its former orientation together with the rigid-body rotation. This sequence is repeated for every increment of matrix deformation until a chosen finite deformation is reached. For this purpose, the pure shear increments ($\Delta\varepsilon_x$) are added to yield the finite logarithmic pure shear (ε_x), and the simple shear increments ($\Delta\gamma_x$) are added to yield the finite simple shear (γ_x).

The deformation simulated by this program is a steady-state flow with constant strain increments. This means that there is no spin of the external foliation in relation to the bulk strain axes and no dynamic change of flow. For less complex strain situations ($D = 1$, $D = 0$, $S_r = 0, S_r = \infty$), the program is checked by the analytic equations of Cox (1971) and Ramsay & Huber (1983, pp. 289–292).

Figures 5–7 illustrate three examples for antithetic rotations of the internal foliation calculated by PROGDEF (θ_a = TETA, θ_{si} = TETSI).

Figure 5 shows the simple shear deformation of a horizontally oriented microlithon with no competency contrast relative to the matrix ($D = 1$). In Fig. 5(a) with the internal deformation being non-coaxial, the ellipse acts like a passive marker; there is no antithetical rotation of the internal foliation. In Fig. 5(b) with the internal deformation being coaxial, however, the internal foliation rotates antithetically.

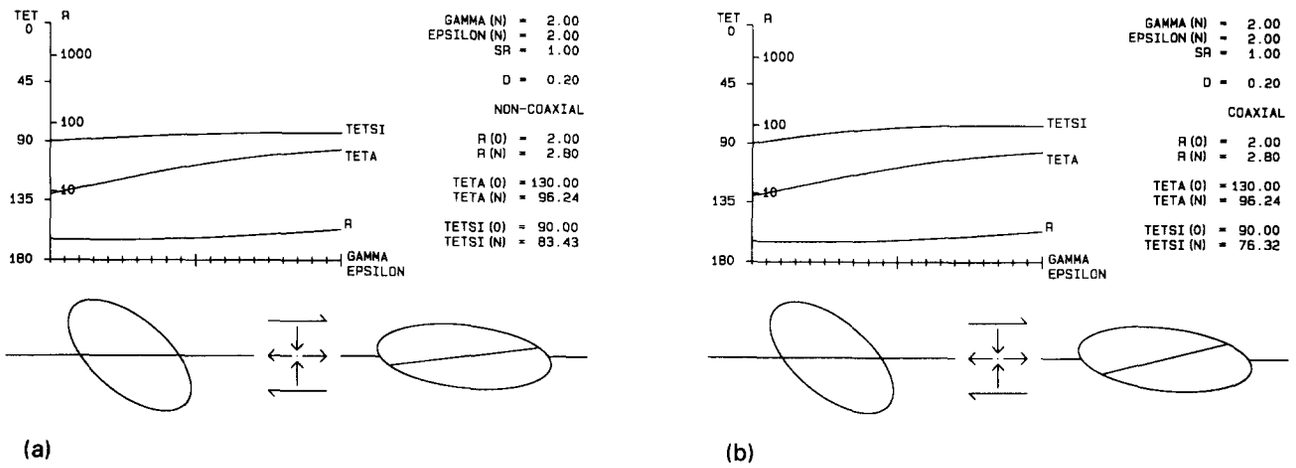

Fig. 6. Combined simple and pure shear deformation of an inclined and relatively competent microlithon. (a) Non-coaxial internal deformation. (b) Coaxial internal deformation.

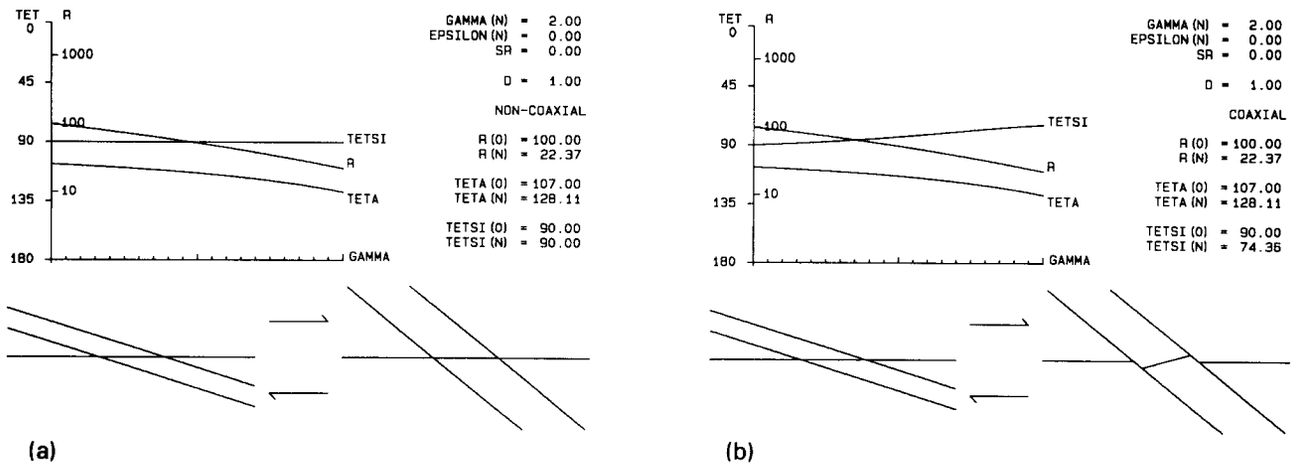

Fig. 7. Simple shear deformation of an incompetent Riedel structure. (a) Non-coaxial internal deformation. (b) Coaxial internal deformation.

Figure 6 shows the combined simple and pure shear deformation and rotation of an inclined and relatively competent ($D = 0.2$) microlithon. This example is most likely for real asymmetric shear band structures. In Fig. 6(a) (non-coaxial internal deformation) an antithetical rotation of both the microlithon and the foliation is seen. It results from the rigid-body rotation of the microlithon which is caused by the extensional pure shear component. In Fig 6(b) this effect is amplified by the coaxial internal deformation.

Figure 7 shows the simple shear deformation of a Riedel structure (initial angle of 17° with the shear plane) with no competency contrast ($D = 1$) and rotating like a passive marker ($R = 100$). Although the boundary shears rotate synthetically, the internal foliation in Fig. 7(b) (coaxial internal deformation) rotates antithetically.

NUMERICAL APPLICATION: STRAIN CALCULATION

A further program, STRAIN, allows the calculation of finite strains from real asymmetric shear band structures. It is a modification of the program PROGDEF and needs as input data the final ellipticity (R_N) and the orientation (θ_{aN}) of the real microlithon, the final orientation of its internal foliation (θ_{siN}) and the measurable logarithmic change of length (ε_z) of the external foliation

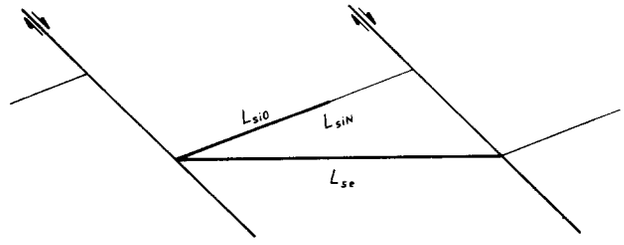

Fig. 8. Changes of length in a shear band structure. Initial length of the internal and external foliation, L_{si0}; final length of the internal foliation, L_{siN}; final length of the external foliation, L_{se}.

with respect to the internal foliation. In Fig. 8, L_{siN} is the final length of the internal foliation and L_{se} is the length it would have outside the microlithon and still being parallel to the external foliation. Both lengths can be roughly measured from real shear band structures and yield ε_z using the following equation:

$$\varepsilon_z = \ln\left(1 + \frac{L_{se} - L_{siN}}{L_{siN}}\right). \tag{5a}$$

Inside the microlithon, the logarithmic change of length (ε_{si}) of the internal foliation with respect to its original length (L_{si0}) is:

$$\varepsilon_{si} = \ln\left(1 + \frac{L_{siN} - L_{si0}}{L_{si0}}\right). \tag{5b}$$

It has to be calculated numerically by:

$$\varepsilon'_{si} = D(\tfrac{1}{2}\gamma'_x \sin 2\theta_{si} - \varepsilon'_x \cos 2\theta_{si}) \tag{5c}$$

for the non-coaxial internal deformation, or by:

$$\varepsilon'_{si} = \varepsilon'_{ai} \cos 2(\theta_{si} - \theta_a) \tag{5d}$$

for the coaxial internal deformation. The sum of both changes of lengths ($\varepsilon_z + \varepsilon_{si}$) is equal to the finite pure shear component (ε_x) parallel to the external foliation which is the total horizontal change of length during the entire deformation:

$$\varepsilon_x = \ln\left(1 + \frac{L_{se} - L_{si0}}{L_{si0}}\right) = \varepsilon_z + \varepsilon_{si}. \tag{5e}$$

Only the relative deformability of the microlithon cannot be measured and has to be estimated. The program proceeds iteratively, based on the conditions that the initial orientation of the internal foliation is equal to that of the external foliation ($\theta_{si0} = \theta_{se} = 90°$) and that the sum of the changes of length of the internal foliation is equal to the finite pure shear (equation 5e).

Output data are the values for finite dextral simple shear (γ_x), for finite logarithmic extensional pure shear (ε_x), for strain-type ratio ($S_r = \varepsilon_x\gamma_x$), for initial ellipticity (R_0) and orientation (θ_{a0}) of the microlithon, and for

initial orientation ($\theta_{si0} = 90°$) and finite logarithmic change of length (ε_{si}) of the internal foliation.

In the following section, the strain calculation for a shear band structure observed in the southern Gurktal Nappe (Eastern Alps, Austria) is presented. The investigated outcrop is located at the Krobathen mountain (Feldkirchen, Carinthia) showing a brittle–ductile shear zone with a duplex structure in the Murau Limestone (Fig. 9) The sense of shear of the duplex is dextral and easterly directed. Below the duplex structure and within the unfaulted and strongly foliated limestone, several asymmetric shear band structures are developed. Figure 10 shows one of these structures with a component dolomitic layer being cut by shear bands and, as shown by the above situated duplex structure, indeed rotated antithetically.

Table 1 gives the finite strain calculations for this shear band structure. Negative values of γ_x indicate a synthetic fabric rotation. Although the microlithons must have been rather undeformable ($D = 0.1$), the calculations were also executed for larger deformabilities just to demonstrate the effect of different deformabilities. But even for $D = 0.1$, an antithetic rotation of the internal foliation results. Further, a finite strain of $\gamma_x = 0.6$ for the simple shear component and of $\varepsilon_x = 0.6$ for the extensional logarithmic pure shear component is calculated. This is equivalent to a dextral shear angle of 31° and to an elongation of 82% in the x-direction. The strain-type ratio amounts to $S_r = \varepsilon_x/\gamma_x = 1$. Strain calculations for other asymmetric shear band structures give similar results.

Table 1. Strain calculations for the Krobathen shear band structure shown in Fig. 10

Data measured from the shear band structure in Fig. 10

R_N	θ_{aN}	θ_{siN}	ε_z
2.9	108.0	80.0	0.53

Calculated data

D	R_0	θ_{a0}	θ_{si0}	ε_{si}	γ_x	ε_x	S_r
(a) *For non-coaxial internal deformation*:							
0.0	2.9	118.0	90.0	0.00	0.54	0.53	0.98
0.1	2.8	121.7	90.0	0.06	0.56	0.59	1.06
0.2	2.7	126.7	90.0	0.14	0.57	0.67	1.18
0.3	2.7	133.7	90.0	0.24	0.54	0.77	1.43
0.4	2.7	143.7	90.0	0.37	0.44	0.90	2.04
0.5	2.9	157.8	90.0	0.52	0.18	1.05	5.85
0.6	3.6	177.3	90.0	0.68	−0.41	1.21	−2.97
(b) *For coaxial internal deformation*:							
0.0	2.9	118.0	90.0	0.00	0.54	0.53	0.98
0.1	2.8	119.7	90.0	0.01	0.55	0.54	0.98
0.2	2.7	121.4	90.0	0.01	0.57	0.54	0.95
0.3	2.7	122.8	90.0	0.02	0.62	0.55	0.88
0.4	2.8	123.7	90.0	0.01	0.70	0.54	0.78
0.5	2.9	123.5	90.0	0.00	0.84	0.53	0.63
0.6	3.3	121.4	90.0	−0.03	1.11	0.50	0.45
0.7	4.3	115.7	90.0	−0.11	1.62	0.42	0.26
0.8	8.1	104.3	90.0	−0.38	2.84	0.16	0.06

DISCUSSION AND CONCLUSION

It has been shown that combined simple and pure shear will cause antithetical fabric rotations in shear band structures if the bulk strain is further partitioned into rigid-body rotation and reduced internal deformation. Simple shear without any foliation-parallel pure shear will also produce antithetical fabric rotation if a reduction of the shear-induced vorticity inside the shear band structures takes place.

Strain calculations from real asymmetric shear band structures have shown that these structures must have developed in combined simple shear and extensional pure shear with the internal foliation being rotated antithetically. For small relative deformabilities of the microlithons ($D = 0.1$ to $D = 0.3$), the calculated finite simple shear (γ_x) amounts to 0.5–0.6, and the extensional logarithmic pure shear (ε_x) amounts to 0.3–0.6.

The strain model presented above is a kinematic one which is only based on geometrical constraints. It does not include physical parameters such as stress, viscosity and friction, and even the development of new shear planes is not considered. But it describes sufficiently well the range of deformation types—from rigid-body rotation to non-coaxial and coaxial internal strain—that enable antithetical fabric rotations.

The main problem of the model is that a single elliptic microlithon in a homogeneous matrix has been assumed rather than a rhombic one surrounded by other microlithons. Adjoining microlithons will change the rotation rates given by equation (2) because otherwise gaps and overlaps would occur and strain would not be compatible. The same rule should apply to other inhomogeneities of the embedding matrix. But following Bretherton (1962) and Passchier (1987), the rotation of nearly rhombic microlithons is not very different from elliptic ones. And following Tullis (1976), who investigated experimentally the deformation of micas, a matrix consisting of numerous microlithons only slows down the rotation rate but does not change its sense.

Thus, the model is suitable to determine the sense of rotation of a given structure and to decide whether it is, for example, an antithetically rotated shear band structure or a synthetically rotated bookshelf structure (Ramsay & Huber 1987, p. 633).

The finite simple shear of about 0.6—as calculated from real shear band structures—is very small for shear zones. And the additional pure shear poses problems for the strain compatibility because it is not homogeneous over the entire shear zone. But shear band structures are typical for brittle–ductile and brittle deformations with most of the simple shear being partitioned into discrete slips on foliation-parallel shear planes (see Fig. 2b). So the calculated simple shear might be only a minimum, sufficient to determine the sense of shear of the bulk deformation. And the extensional logarithmic pure shear of about 0.6 might be only a local deviation from the mean simple shear since it is caused by heterogeneities in the deforming rock. Even duplex structures represent a local—compressive—pure shear in addition

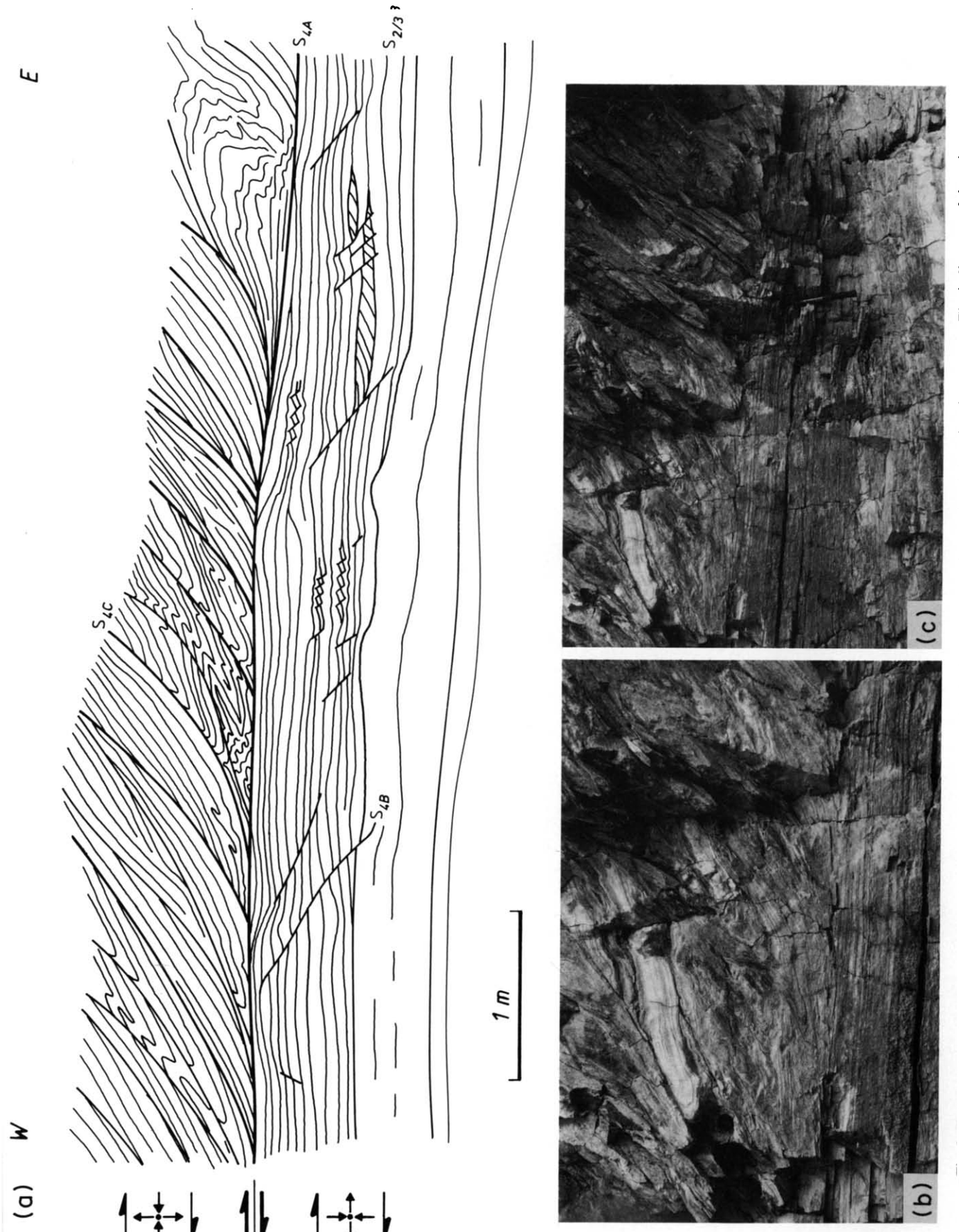

Fig. 9. The Krobathen shear zone in Murau Limestone with a compressive duplex structure and extensional shear band structures. The bulk sense of shear is dextral and indicates a late eastward transport of the Gurktal Nappe.

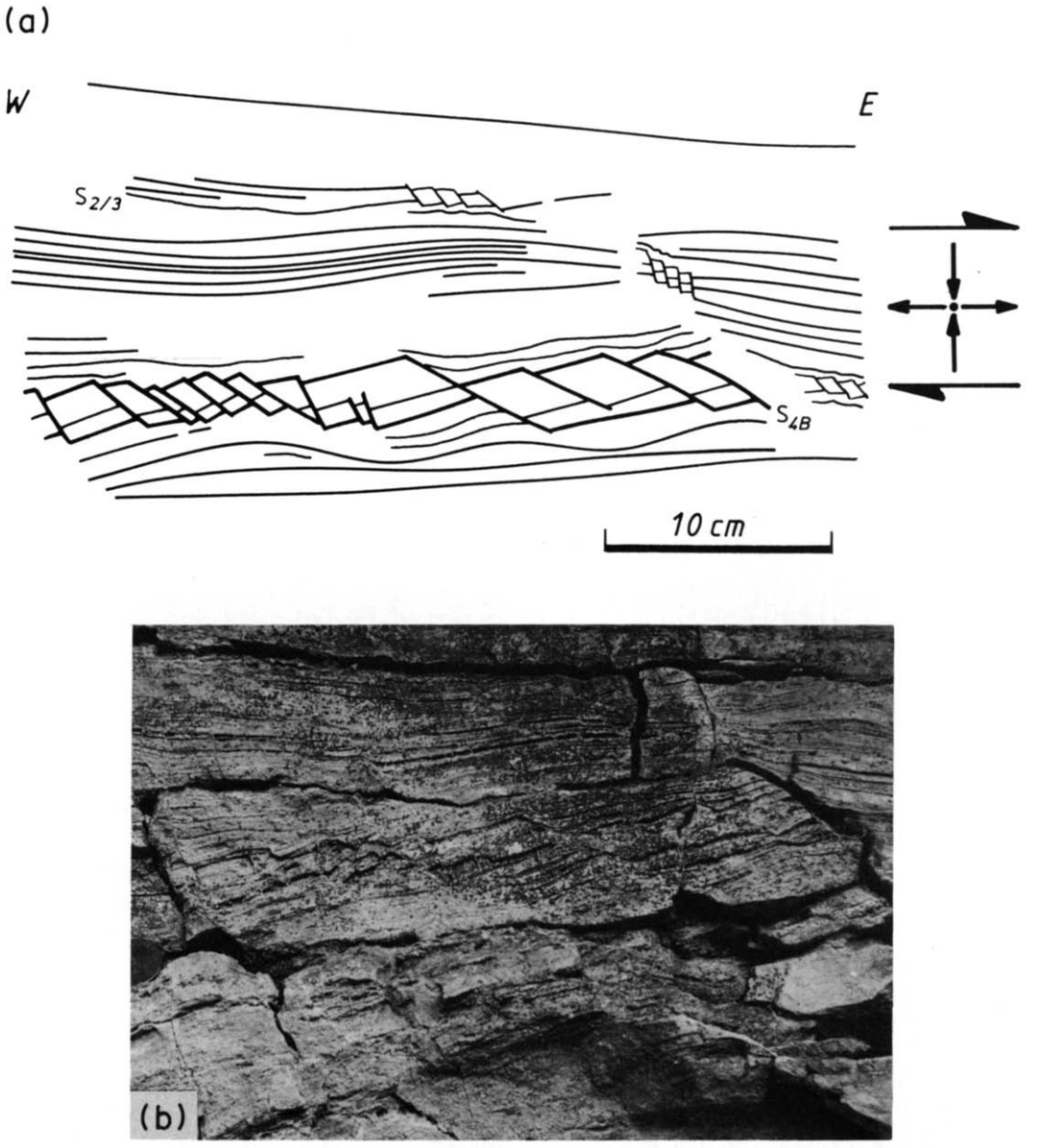

Fig. 10. A single shear band structure of the Krobathen shear zone. Below the duplex structure, a competent dolomitic layer is cut by brittle shear bands. The microlithons are rotated antithetically with respect to the bulk sense of shear.

to the major simple shear, and their coexistence with extensional shear band structures in one and the same shear zone is not contradictional as seen in Fig. 9 or as described by Platt & Leggett (1986).

Acknowledgements—I would like to thank J. H. Behrmann and D. M. Ragan who reviewed this paper in a very constructive way.

REFERENCES

Behrmann, J. H. 1987. A precautionary note on shear bands as kinematic indicators. *J. Struct. Geol.* **9**, 659–666.

Bretherton, F. P. 1962. The motion of rigid particles in a shear flow at low Reynolds number. *J. Fluid. Mech.* **14**, 284–304.

Cox, R. G. 1971. The motion of long slender bodies in a viscous fluid. 2, Shear flow. *J. Fluid. Mech.* **45**, 625–657.

Ghosh, S. K. & Ramberg, H. 1976. Reorientation of inclusions by combination of pure shear and simple shear. *Tectonophysics* **34**, 1–70.

Hanmer, S. K. 1986. Asymmetrical pull-aparts and foliation fish as kinematic indicators. *J. Struct. Geol.* **8**, 111–121.

Harris, L. B. & Cobbold, P. R. 1984. Development of conjugate shear bands during bulk simple shearing. *J. Struct. Geol.* **7**, 37–44.

Lister, G. S. & Williams, P. F. 1983. The partitioning of deformation in flowing rock masses. *Tectonophysics* **92**, 1–33.

Means, W. D. 1976. *Stress and Strain*. Springer, New York.

Means, W. D., Hobbs, B. E., Lister, G. S. & Williams, P. F. 1980. Vorticity and non-coaxility in progressive deformation. *J. Struct. Geol.* **2**, 371–378.

Passchier, C. W. 1984. The generation of ductile and brittle shear bands in a low angle mylonite zone. *J. Struct. Geol.* **6**, 273–281.

Passchier, C. W. 1987. Stable positions of rigid objects in non-coaxial flow—a study in vorticity analysis. *J. Struct. Geol.* **9**, 679–690.

Platt, J. P. 1979. Extensional crenulation cleavage. *J. Struct. Geol.* **1**, 95–96.

Platt, J. P. 1984. Secondary cleavages in ductile shear zones. *J. Struct. Geol.* **6**, 439–442.

Platt, J. P. & Leggett, J. K. 1986. Stratal extension in thrust footwalls, Makran Accretionary Prism: implications for thrust tectonics. *Bull. Am. Ass. Petrol. Geol.* **70**, 191–203.

Platt, J. P. & Vissers, R. L. M. 1980. Extensional structures in anisotropic rocks. *J. Struct. Geol.* **2**, 397–410.

Ramsay, J. G. & Huber, M. I. 1983. *The Techniques of Modern Structural Geology, Volume* 1: *Strain Analysis*. Academic Press, London.

Ramsay, J. G. & Huber, M. I. 1987. *The Techniques of Modern Structural Geology, Volume* 2: *Folds and Fractures*. Academic Press, London.

Stock, P. 1989. Zur antithetischen Rotation der Schieferung in Scherbandgefügen—ein kinemtaisches Deformationsmodell mit Beispielen aus der südlichen Gurktaler Decke (Ostalpen). *Frankfurter geowiss. Arb.*, **A7**.

Tullis, T. E. 1976. Experiments on the origin of slaty cleavage and schistosity. *Bull. geol. Soc. Am.* **87**, 745–753.